Seasonal variations in the sources of organic aerosol in Xi'an, Northwest China: The importance of biomass burning and secondary formation

Haobin Zhong, Ru-Jin Huang, Jing Duan, Chunshui Lin, Yifang Gu, Ying Wang, Yongjie Li, Yan Zheng, Qi Chen, Yang Chen, Wenting Dai, Haiyan Ni, Yunhua Chang, Douglas R. Worsnop, Wei Xu, Jurgita Ovadnevaite, Darius Ceburnis, Colin D. O'Dowd

PII: S0048-9697(20)33186-7

DOI: https://doi.org/10.1016/j.scitotenv.2020.139666

Reference: STOTEN 139666

To appear in: *Science of the Total Environment*

Received date: 2 April 2020

Revised date: 22 May 2020

Accepted date: 22 May 2020

Please cite this article as: H. Zhong, R.-J. Huang, J. Duan, et al., Seasonal variations in the sources of organic aerosol in Xi'an, Northwest China: The importance of biomass burning and secondary formation, *Science of the Total Environment* (2020), https://doi.org/10.1016/j.scitotenv.2020.139666

Seasonal variations in the sources of organic aerosol in Xi'an, Northwest China: the importance of biomass burning and secondary formation

Haobin Zhong[1,2], Ru-Jin Huang[1,3], Jing Duan[1,2], Chunshui Lin[1], Yifang Gu[1,2], Ying Wang[1,2], Yongjie Li[4], Yan Zheng[5], Qi Chen[5], Yang Chen[6], Wenting Dai[1], Haiyan Ni[1], Yunhua Chang[7], Douglas R. Worsnop[8], Wei Xu[1,9], Jurgita Ovadnevaite[9], Darius Ceburnis[9], Colin D. O'Dowd[9]

[1]State Key Laboratory of Loess and Quaternary Geology (SKLLQG), Center for Excellence in Quaternary Science and Global Change, and Key Laboratory of Aerosol Chemistry and Physics, Institute of Earth Environment, Chinese Academy of Sciences, Xi'an 710061, China
[2]University of Chinese Academy of Sciences, Beijing 100049, China
[3]Institute of Global Environmental Change, Xi'an Jiaotong University, Xi'an 710049, China
[4]Department of Civil and Environmental Engineering, Faculty of Science and Technology, University of Macau, Taipa, Macau 999078, China
[5]State Key Joint Laboratory of Environmental Simulation and Pollution Control, College of Environmental Sciences and Engineering, Peking University, Beijing 100871, China
[6]Chongqing Institute of Green and Intelligent Technology, Chinese Academy of Sciences, Chongqing 400714, China
[7]Yale-NUIST Center on Atmospheric Environment, Nanjing University of Information Science & Technology, Nanjing 210044, China
[8]Aerodyne Research, Inc., Billerica, MA, USA
[9]School of Physics and Centre for Climate and Air Pollution Studies, Ryan Institute, National University of Ireland Galway, University Road, Galway H91CF50, Ireland
Correspondence to: Ru-Jin Huang (rujin.huang@ieecas.cn)

Abstract

The Guanzhong basin is a part of the three top priority regions in China's blue sky action as of 2019. Understanding the chemical composition, sources, and atmospheric process of aerosol in this region is therefore imperative for improving air quality. In this study, we present, for the first time, the seasonal variations of organic aerosol (OA) in Xi'an, the largest city in the Guanzhong basin. Biomass burning OA (BBOA) and oxidized OA (OOA) contributed > 50% of OA in both autumn and winter. The average concentrations of BBOA in autumn (14.8 ± 5.1 μg m^{-3}) and winter (11.6 ± 6.8 μg m^{-3}) were similar. The fractional

contribution of BBOA to total OA, however, decreased from 31.9% in autumn to 15.3% in winter, because of enhanced contributions from other sources in winter. The OOA fraction in OA increased largely from 20.9% in autumn to 34.9% in winter, likely due to enhanced emissions of precursors and stagnant meteorological conditions which facilitate the accumulation and secondary formation. A large increase in OOA concentration was observed during polluted days, by a factor of ~4 in autumn and ~6 in winter compared to clean days. In both seasons, OOA formation was most likely dominated by photochemical oxidation when aerosol liquid water content was less than 30 μg m^{-3} or by aqueous-phase processes when O_x was less than 35 ppb. A higher concentration of BBOA was observed for air masses circulated within the Guanzhong basin (16.5-18.1 μg m^{-3}), compared to air masses from Northwest and West (10.9-14.5 μg m^{-3}). Furthermore, compared with OA fraction in non-refractory PM_1 in other regions of China, BBOA (17-19%) and coal combustion OA (10-20%) were major emission sources in the Guanzhong Basin and the BTH region, respectively, whereas OOA (10-34%) was an important source in all studied regions.

Key Words: Haze pollution; the Guanzhong basin; biomass burning; secondary organic aerosol.

1 Introduction

The rapid economic development, industrialization and urbanization in China have led to severe particulate air pollution particularly in northern China which, consequently, affects air

quality, human health, ecosystem, regional and global climate (Tie et al., 2016; Cohen et al., 2017; An et al., 2019). These severe particulate pollution events are often accompanied by high emissions of primary aerosol and secondary aerosol precursors from multiple sources, large secondary aerosol formation, regional transport, unfavorable meteorological and climatic conditions, as well as their synergetic effects (An et al., 2019). Quantitative understanding of the chemical composition, sources, and atmospheric processes of aerosol is therefore crucial for mitigating the particulate air pollution.

Numerous studies have been carried out in the past years to improve the scientific understanding of particulate air pollution, especially in the Beijing-Tianjin-Hebei (BTH) region. In particular, online measurements with Aerodyne aerosol mass spectrometer (AMS) and aerosol chemical speciation monitor (ACSM) have greatly improved our understanding in the chemical nature, sources, and evolution of aerosol (Sun et al., 2013a; Sun et al., 2016a; Elser et al., 2016; Wang et al., 2017; Duan et al., 2019; Huang et al., 2019). For example, previous studies in Beijing show that high mass concentration of NR-PM_1 is related to the growth of secondary inorganic aerosol, accompanied by the increased relative humidity (Sun et al., 2013a). Coal combustion has also been identified as the main contributor to OA mass (about 24-48%) in Beijing (Sun et al., 2013a; Hu et al., 2016; Elser et al., 2016). In other cities of the BTH region, for example, in Shijiazhuang, the capital city of Hebei province, Huang et al., (2019) illustrated that sulphate accounted for a significant fraction (24%) of NR-PM_1 (74.4 μg m^{-3}) in the extremely polluted days. Similar to Beijing, coal combustion was also found to be the main source of OA in Shijiazhuang (25%, Huang et al., 2019) and Handan (29%, Li et al., 2017).

Different from the BTH region, online characterization of aerosol in the Guanzhong basin is still very limited. A noticeable geographical difference in the emission sources between the BTH region and the Guanzhong basin has been observed, with residential coal combustion and biomass burning as a major emission source in the BTH region and the Guanzhong basin, respectively (Elser et al., 2016; Wang et al., 2017). The particulate air pollution in the Guanzhong basin is also very severe and therefore this basin (as a part of the Fenwei plain) is listed as one of three regions of the highest priority in China's air pollution mitigation plan.

As the largest city of the Guanzhong basin, Xi'an has suffered from severe particulate pollution over the past decades. The average annual concentrations of $PM_{2.5}$ range from 50.6-170 μg m^{-3} in Xi'an from 2004-2016 (Xu et al., 2017; Liu et al., 2019). However, the chemical nature and sources leading to such high particulate pollution in Xi'an are not well characterized. Most of the previous studies are based on offline analysis of certain chemical composition on filter samples or conducted over a short period (Wang et al., 2015a; Dai et al., 2018), limiting our understanding of the cause of particulate pollution in Xi'an. Long-term and real-time measurements are therefore crucial to obtain new insights into the chemical composition, sources, and atmospheric processes of aerosol in this region.

In this study, we investigate the chemical nature of non-refractory PM_1 in Xi'an during autumn and winter using a quadrupole aerosol chemical speciation monitor (Q - ACSM). The sources and atmospheric evolution of OA are studied, together with the effects of meteorological conditions and air masses.

2 Experimental

2.1 Sampling site and instrumentation

Field measurements were carried out on the rooftop of the building, about 10 m above the ground, at the campus of the Institute of Earth Environment, Chinese Academy of Sciences (34°23′N, 108°89′) from 1 Oct. 2012 to 21 Feb. 2013. The sampling site was surrounded by residential, commercial and traffic area. A quadrupole ACSM (Aerodyne Research Inc., Billerica, MA, US) was deployed for continuous measurements of non-refractory PM_1 species including organics, sulfate, nitrate, ammonium, and chloride. The time resolution was 15 min for the continuous measurements. Ambient air was drawn through a 3/8-inch stainless steel tube at a flow rate of 3 L min^{-1}, and the coarse particles were removed by a cyclone (2.5 μm size cut, URG-2000-30ED) in front of the sampling inlet. The sampled air was dried by a Nafion dryer (MD-110-48S, Perma Pure, Inc., Lakewood, NJ, US) before entering into the ACSM. The aerosol beam was concentrated by an aerodynamic lens and transported to a vaporizer at 600^{o}C for evaporation and further ionization by electron impact, and then the resulting ion fragments were determined by the quadrupole mass spectrometer. In addition, a scanning mobility particle sizer (SMPS, TSI model 3080) with a differential mobility analyzer and a condensation particle counter (CPC, TSI model 3772) were combined for the calibration of ionization efficiency (IE) and relative ionization efficiency (RIEs). CO, SO_2, NO_x and O_3 were measured by the gas analyzers (Thermo Scientific Inc.). Meteorological data (temperature, RH, wind speed and wind direction) were measured by an automatic weather station (MAWS201, Vaisala, Vantaa, Finland) and a wind sensor (Vaisala Model

QMW101-M2). Filter samples were collected 3 meters away from the ACSM by a mini-volume aerosol sampler (Airmetrics, Oregon, US), providing 24-hr integrated $PM_{2.5}$ mass concentrations for comparison purposes.

2.2 Data analysis

The ACSM DAQ software 1.4.4.5 (Aerodyne Research Inc., Billerica, MA, US) was used for acquisition and ACSM local tool version 1.5.3.5 (Aerodyne Research Inc., Billerica, MA, US) in Igor Pro 6.37 (WaveMetrics, Inc., Lake Oswego, Oregon, US) was used for ACSM data analysis and PMF matrices export. Organics, nitrate and chloride were analyzed using the standard RIEs which were 1.4, 1.1 and 1.3, respectively (Canagaratna et al., 2007). RIEs of ammonium (6.47) and sulphate (1.2) were estimated from IE and RIE calibrations. The composition dependent collection efficiency was calculated following the procedure described in Middlebrook et al., (2012).

The source apportionment of organic aerosol was performed by positive matrix factorization (PMF, Paatero and Tapper, 1994; Paatero, 1997) and multilinear engine (ME-2, Paatero, 1999). PMF and ME-2 analysis were performed on the interface of SoFi (version 6.3, Canonaco et al, 2013). PMF is a bilinear receptor model which separates the input data matrix to distinct source factors and their corresponding time-dependent concentrations. However, unconstrained PMF may lead to unclear separation or a mixture of factors due to the rotational ambiguity, especially in the environment with multiple emission sources and complex atmospheric processes, such as the Guanzhong basin. ME-2 provides a restriction method where *a priori* factor profile or time series is used to direct the apportionment results

to an environmentally meaningful solution. The *a* value approach was applied to constrain one or more factor profiles by giving a constrained range. To minimize the influence of non-local input profiles, the constrained range of *a* value is optimally selected (Huang et al., 2019; Duan et al., 2019). The details of the factor-selection and constraining strategies using SoFi are presented in section S1 of the supplementary.

2.3 Aerosol liquid water content

The aerosol liquid water content (ALWC) is calculated using the ISORROPIA-Ⅱ model (Fountoukis and Nenes, 2007). The inorganic aerosol composition from ACSM, together with the temperature and RH, was used as the model inputs, and the ALWC was calculated based on the NH_4^+-SO_4^{2-}-NO_3^--Cl^--H_2O system in thermodynamic equilibrium. In this study, "forward" mode was used in ISORROPIA-Ⅱ, in which both gaseous and particle species were calculated as model inputs. Meanwhile, we used "metastable" mode in our run, where the particles are considered as deliquescent with no solid formation (Fountoukis and Nenes, 2007).

2.4 Trajectory analysis

The trajectory analysis in two seasons were performed by the HYSPLIT model (Draxler and Hess, 1998) in TrajStat which is an integrated software with some trajectory statistics functions (TrajStat_v1.2). Briefly, trajectories were calculated per hour from meteorological data which was available from HYSPLIT (http://www.arl.noaa.gov/ready/hysplit4.html) with 72 hours back at a height of 500 m. In our results, 1072 trajectories in autumn and 2361 trajectories in winter were calculated and they were clustered using the Cluster Analysis and

Cluster Statistics module in TrajStat. Three clusters are the most appropriate results for both autumn and winter.

3 Results and discussion

3.1 Characteristics and seasonal difference of NR-PM_1

Figure 1 shows the time series of NR-PM_1 composition. The average mass concentration of NR-PM_1 was 139 ± 92.8 μg m^{-3}, ranging from 1.2 μg m^{-3} to 497 μg m^{-3}. The mass concentration of NR-PM_1 was well correlated with that of $PM_{2.5}$ (R^2 = 0.8). The slope of 0.7 between NR-PM_1 and $PM_{2.5}$ indicated NR-PM_1 accounted for about 70% of the $PM_{2.5}$ mass (Figure S6). Organic was the dominant NR-PM_1 component (53.5%; 76.1 μg m^{-3}), followed by sulphate (15.8%, 22.0 μg m^{-3}), nitrate (13.0%, 18.1 μg m^{-3}), ammonium (12.3%, 17.1 μg m^{-3}) and chloride (5.3%, 7.4 μg m^{-3}). The average concentration of NR-PM_1 measured in this study is much higher than that in many other cities in China measured in autumn and winter close to our measurement period (± 2 years). For example, it was twice higher than that in Baoji (54 μg m^{-3}, Wang et al., 2017) and Beijing (66.8 μg m^{-3}, Sun et al., 2013b), 2-6 times higher than that in the southeastern cities of China, such as Hong Kong (25.9 μg m^{-3}, Sun et al., 2016b), Nanjing (89.3 μg m^{-3}, Zhang et al., 2015a), Lin'an (63 μg m^{-3}, Zhang et al., 2015b), and 11 times higher than in the western cities of China, such as Tibetan Plateau (11.4 μg m^{-3}, Du et al., 2015).

The seasonal comparisons of NR-PM_1 chemical composition and OA factors between autumn and winter are shown in Fig. S5, and their mass concentrations are shown in Table S1. Organics were the most abundant component in NR-PM_1 in both seasons with the mass

fractions of 58.3% in autumn and 52.2% in winter, respectively. Although the proportion of organics decreased from autumn to winter, the mass concentration increased from 53.9 ± 35.9 μg m^{-3} to 84.2 ± 56.1 μg m^{-3}. Sulphate showed a remarkable increase from 11.6% (10.7 ± 8.5 μg m^{-3}) in autumn to 16.8% (27.1 ± 21.7 μg m^{-3}) in winter. Nitrate decreased from 14.9% in autumn to 12.6% in winter but the corresponding mass concentration increased from 13.8 ± 10.7 μg m^{-3} to 20.3 ± 12.6 μg m^{-3}. Ammonium increased from 10.2% (9.4 ± 7.0 μg m^{-3}) in autumn to 13% (21.0 ± 16.3 μg m^{-3}) in winter and chloride increased from 4.8% (4.3 ± 4.9 μg m^{-3}) in autumn to 5.2% (8.7 ± 6.9 μg m^{-3}) in winter. In autumn, nitrate was the major inorganic species, while in winter sulphate became the most important component of inorganic species. This is consistent with measurements from other northern cities of China. For example, the study in Beijing showed high sulphate to nitrate ratio in winter due to the contribution of coal combustion (Wang et al., 2015b).

3.2 Primary and secondary organic aerosol

The source apportionment results of OA show that BBOA and OOA were the dominant OA source in autumn and winter respectively. BBOA constituted 31.9% (14.8 ± 5.1 μg m^{-3}) of total OA in autumn but decreased to 15.3% (11.6 ± 6.8 μg m^{-3}) in winter. In contrast, OOA fraction of OA increased from 20.9% (9.7 ± 4.1 μg m^{-3}) in autumn to 34.9% (26.5 ± 10.4 μg m^{-3}) in winter. The abundant BBOA in autumn is attributed to the biomass burning activities in the surrounding areas of Xi'an (like agricultural waste or residential fuel combustion). This is consistent with the fact that in the rural areas of Guanzhong basin, straws were widely used for heating and cooking from early September following the harvest. In winter, the

concentrations of BBOA decreased slightly, from 14.8 ± 5.1 μg m^{-3} in autumn to 11.6 ± 6.8 μg m^{-3} in winter, but its fractional contribution to OA decreased to about half, from 31.9% to 15.3%. Meanwhile, the contribution of CCOA increased from 10.4% (4.8 ± 2.6 μg m^{-3}) in autumn to 13.4% (10.2 ± 4.4 μg m^{-3}) in winter, but still lower than that of BBOA. To minimize the effect of planetary boundary layer (PBL) heights, the data were further normalized by ΔCO because CO is often used to account for dilution on timescales of hours to days due to its long lifetime against oxidation by OH radicals (DeCarlo et al., 2010). After offsetting the PBL dilution effect, the time series of BBOA/ΔCO showed a twofold reduction from autumn to winter (Figure S7). The average ratio of BBOA/ΔCO was 25.4 ± 10.7 μg m^{-3} ppm^{-1} in autumn and decreased to 11.2 ± 10.5 μg m^{-3} ppm^{-1} in winter, illustrating that the emissions of BBOA were indeed higher in autumn. HOA contributed 20.5% of OA (9.5 ± 6.4 μg m^{-3}) in autumn and 23.2% of OA (17.6 ± 12.3 μg m^{-3}) in winter. This is consistent with previous studies during winter in Xi'an (18.8%, Elser et al., 2016) and Baoji (20% Wang et al., 2017). The mass concentrations of COA were 7.6 ± 2.2 μg m^{-3} (16.4%) in autumn and 9.8 ± 3.7 μg m^{-3} (13.1%) in winter, indicating that emissions from cooking activities are relatively stable in different seasons (Sun et al., 2018).

To understand the role of photochemical oxidation versus aqueous-phase processes in SOA (OOA is a surrogate of SOA in our study) formation, the relationships between the fraction of OOA in OA (f_{OOA}) and odd oxygen ($O_x = O_3 + NO_2$) or aerosol liquid water content (ALWC) were investigated. Figure 2 shows the scatter plot of hourly averaged f_{OOA} versus O_x (a) and ALWC (b) during daytime (from 7:00 to 18:00, local time) in autumn and winter. In autumn, the O_x concentrations ranged from 28.9 ppb to 55.0 ppb and f_{OOA} ranged from 4% to 33%.

When ALWC < 30 μg m^{-3}, we found that f_{OOA} was well correlated with O_x (R^2 = 0.67), increasing from 6% to 23% as the O_x concentrations increased from 29.4 ppb to 43.4 ppb. In winter, the OOA fraction ranged from 9% to 61%, about twice that in autumn. When ALWC < 30 μg m^{-3}, f_{OOA} also showed a positive correlation with O_x (R^2 = 0.48), increasing from 20% to 38% when the O_x concentrations increased from 25.8 ppb to 40.0 ppb. These results suggest the importance of photochemical oxidation in SOA formation when ALWC less than 30 μg m^{-3} in both autumn and winter. On the other hand, the aqueous-phase processes are likely more important under the condition of low O_x concentrations. In autumn, when O_x < 35 ppb, f_{OOA} increased from 4% to 30% and was well correlated with ALWC (R^2 = 0.83). Also, in winter, f_{OOA} increased from 20% to 58% and was well correlated with ALWC when ALWC < 100 μg m^{-3} and O_x < 35 ppb (R^2 = 0.58). When ALWC > 100 μg m^{-3}, however, f_{OOA} was rather stable at about 40-55% (note that OOA increased with ALWC, see Figure S10), due to enhanced POA accumulation during high pollution episodes (see Figure S10). On the other hand, the poor correlations when O_x > 35 ppb and ALWC > 100μg m^{-3} indicate that both photochemical oxidation and aqueous-phase processes have effects on the OOA formation under this condition.

3.3 Evolution of Chemical species and OA sources at different NR-PM_1 levels

Figure 3 shows the contributions of different NR-PM_1 species and OA factors in the clean, moderately polluted and heavily polluted days, representing the 25th (N=11 in autumn and N=24 in winter), 25-75th (N=23 in autumn and N=48 in winter) and 75th (N=11 in autumn and N=24 in winter) percentiles of daily average NR-PM_1 mass concentrations, respectively. In

autumn, the average mass concentration of NR-PM_1 in heavily polluted days was 169 μg m^{-3}, about ~1.8 and ~3.4 times larger than that in moderately polluted days (93.9 μg m^{-3}) and clean days (49.1 μg m^{-3}), respectively. In winter, the average mass concentration of NR-PM_1 during heavily polluted days (279 μg m^{-3}) was about ~1.7 and ~4 times higher than that in moderately days (161 μg m^{-3}) and clean days (70 μg m^{-3}). The proportion of organics decreased slightly from clean days to heavy pollution days in both autumn (from 59% to 56% of NR-PM_1) and winter (from 56% to 52% of NR-PM_1), but its corresponding mass concentration increased significantly, from 28.9 μg m^{-3} to 94.5 μg m^{-3} in autumn and from 39.2 μg m^{-3} to 145 μg m^{-3} in winter. Also, the mass concentration of secondary inorganic aerosol (SIA, indicates to the sum of sulphate, nitrate and ammonium) increased from 18.2 μg m^{-3} in clean days to 34.7 μg m^{-3} in moderately polluted days and further to 64.1 μg m^{-3} in heavily polluted days in autumn, and correspondingly from 26.6 μg m^{-3} to 69.4 μg m^{-3} and further to 117 μg m^{-3} in winter. Likewise, the mass concentration of SOA increased from 4.4 μg m^{-3} in clean days to 10.1 μg m^{-3} in moderately polluted days and further to 16.8 μg m^{-3} in heavily polluted days in autumn, and correspondingly from 8 μg m^{-3} to 25.3 μg m^{-3} and further to 47.9 μg m^{-3} in winter. These results are consistent with previous studies in the BTH region (Huang et al., 2019; Duan et al., 2019), suggesting that the pollution events are largely promoted by enhanced secondary aerosol formation, besides contributions from POA. Of note, nitrate showed a significant increase from 12% (5.9 μg m^{-3}) in clean days to 15% (14.1 μg m^{-3}) in moderately polluted days, and further to 17% (28.7 μg m^{-3}) in heavily polluted days in autumn. On the contrary, in winter, sulphate increased from 13% (9.1 μg m^{-3}) in clean days to 17% (27.4 μg m^{-3}) in moderately polluted days and further to 18% (50.1 μg m^{-3}) in heavily

polluted days. In terms of OA sources, BBOA was the abundant POA persistently in all mass concentration levels (accounting for 31-33% of OA) and its mass concentration increased from 8 μg m^{-3} in clean days to 14.7 μg m^{-3} in moderately polluted days and further to 24.8 μg m^{-3} in heavily polluted days in autumn, indicating the primary emission from biomass burning also played an important role to the pollution events. HOA increased from 3.6 μg m^{-3} to 8.3 μg m^{-3} and further to 20.8 μg m^{-3} in autumn and from 6.0 μg m^{-3} to 15.9 μg m^{-3} and further to 32.8 μg m^{-3} in winter from clean days to moderately polluted days and further to heavily polluted days. Its proportion was about a quarter of total OA mass concentration in heavily polluted days in both autumn and winter, illustrating traffic emission was significant contributor to heavy haze in Xi'an. CCOA increased from 1.9 μg m^{-3} to 4.6 μg m^{-3} and further to 9.6 μg m^{-3} in autumn and from 4.1 μg m^{-3} to 10.1 μg m^{-3} and further to 16.4 μg m^{-3} in winter from clean days to moderately polluted days and further to heavily polluted days. CCOA was an important OA source accounting for ~13% of total OA mass consistently in all pollution levels in winter, whereas, in autumn, it was only significant in heavily polluted days (12%). COA was rather stable at about ~10 μg m^{-3} in all pollution levels in both autumn and winter, and it was only important to OA in clean days (26% in autumn and 22% in winter).

Furthermore, four cases were selected, of which each includes clean, moderately polluted, and heavily polluted events (the time series and detailed information of four cases are available in Figure 1 and Figure S9), to investigate the role of secondary formation in particulate pollution. As shown in Fig. 4 and Table S2, the concentrations of SOA and SIA increased by a factor of 3.5-4.3 and 3.4-4.5, respectively, from clean events to heavily polluted events in all four cases, demonstrating the significance of secondary processes in particulate pollution. However, the

fractional contributions of SOA and SIA show some differences from case to case. Specifically, in autumn, in Case 1, SIA increased from 36.9% to 41.1% of NR-PM_1 and OOA increased from 22.4% to 32.5% of OA from clean to heavily polluted events. In Case 2, however, SIA decreased from 40.0% to 35.8% of NR-PM_1 and OOA decreased from 20.9% to 16.3% of OA from clean to heavily polluted events. Likewise, in winter, in Case 3, SIA increased from 43.9% to 46.9% of NR-PM_1 and OOA increased from 40.4% to 45.9% of OA from clean to heavily polluted events. In Case 4, however, SIA decreased from 40.0% to 33.0% of NR-PM_1 and OOA decreased from 36.6% to 35.1% of OA from clean to heavily polluted events. The difference from case to case is likely due to the difference in meteorological conditions (e.g. wind speed and RH) which affect the formation of secondary aerosol formation and the accumulation/ dilution of aerosol.

3.4 Back trajectory analysis

Figure 5 shows the back trajectory results in autumn and winter, with three clusters in both seasons. In autumn, the major air masses (46%) were from northwest China characterized by long-distance transport and relatively clean air. The mass concentration of NR-PM_1 for the northwest cluster was the lowest (83.1 μg m^{-3}), and OA was the major fraction (62%, or 51.5 μg m^{-3}) with the largest contribution from BBOA (33% of OA, or 14.5 μg m^{-3}). The other two clusters represented the short-distance transport from west of Guanzhong basin (24% of the measurement days) and east of Guanzhong basin (30% of the measurement days). These two clusters had similar mass concentrations and chemical composition (See Figure 5a), indicating that the air masses in the Guanzhong basin were well mixed and representing

similar contribution of sources. It should be noted that both SIA (42% of NR-PM_1 or 48.2 μg m^{-3} for the west; 37% of NR-PM_1 or 40.5 μg m^{-3} for east) and SOA (26% of OA or 14.3 μg m^{-3} for the west; 24% of OA or 14.4 μg m^{-3} for east) for the west and east air masses were much higher than for the northwest air masses (SIA: 31% of NR-PM_1 or 25.8 μg m^{-3}; SOA: 16% of OA or 7 μg m^{-3}), likely due to large emissions of their precursors in the Guanzhong basin. Also, the contribution of BBOA was the largest among the OA sources for different clusters.

In winter, the prevailing air masses were also from northwest China (65%), and the rest was from west of China (20%) and the Guanzhong basin (15%). The northwest and west clusters were from long-distance transport and the Guanzhong cluster was from local emissions and short-distance transport. The average mass concentrations for these three clusters are very similar, indicating that the air pollution was widespread in winter. However, the corresponding chemical composition was different. The concentrations of SIA were higher for the west (75.5 μg m^{-3} or 47% of NR-PM_1) and Guanzhong (84.5 μg m^{-3} or 50% of NR-PM_1) clusters than for the northwest cluster (61.0 μg m^{-3} or 38% of NR-PM_1). However, the concentrations of OOA were slightly higher for the northwest cluster (24.1 μg m^{-3} or 33% of OA) than for the west (21.5 μg m^{-3} or 34% of OA) and Guanzhong (21.0 μg m^{-3} or 28% of OA) clusters. Of note, the concentration of BBOA was higher in the Guanzhong cluster (16.5 μg m^{-3} or 22% of OA) than in the northwest (10.9 μg m^{-3} or 15% of OA) and west (11.4 μg m^{-3} or 18% of OA) clusters.

3.5 Comparison with other Chinese cities

Figure 6 shows the comparison of NR-PM_1 composition and OA sources in different regions of China. These data were measured by AMS/ACSM between 2010 and 2015, close to the measurement period (2012-2013) of our study to minimize the temporal variability in emission sources and thus better representation the spatial differences. Note that the data were gathered in autumn and winter, however, seasonal difference in emissions still existed. As shown in Figure 6, the Guanzhong basin and BTH region were the most polluted regions, with the highest NR-PM_1 concentration of 172 μg m^{-3} in Xi'an of the Guanzhong basin (this study) and 178 μg m^{-3} in Shijiazhuang of the BTH region (Huang et al., 2019). The mass concentrations in most of the Yangtze River Delta (YRD) and Pearl River Delta (PRD) regions were < 50 μg m^{-3} (Huang et al., 2013; Zhang et al., 2015c; Li et al, 2015; Sun et al., 2016b). For most results in the Guanzhong basin and BTH region, organic matter was the largest component, contributing to ~50% of particle mass. However, in the PRD and YRD regions, secondary inorganic aerosol dominated, accounting for 40%-60% of particle mass, suggesting that control of NO_x and SO_2 is particularly important for mitigating particulate pollution in those regions. In terms of OA sources, BBOA was the major primary source in the Guanzhong basin (17-19% of particle mass) and CCOA was the major primary source in the BTH region (10-20% of particle mass). However, these two sources were not resolved in southern China during winter due to the absence of residential heating activities. OOA was a major contributor in almost all regions, with the fractional contribution to NR-PM ranging from 10% to 34%. Note that uncertainties from different PMF/ME-2 studies may differ. For example, (Zheng et al., 2020) reported uncertainties of 20% for POA and 40% for OOA. However, such comparisons can still provide insights into the general difference in sources

and atmospheric processes (e.g., photochemical oxidation and aqueous-phase processes) in different regions.

4. Conclusion

Seasonal variability of organic aerosols were measured in near real-time by an ACSM in Xi'an during autumn and winter. The source apportionment results of OA showed that biomass burning OA (BBOA) and oxidized OA (OOA) were the major sources, accounting for > 50% of OA in both autumn and winter. The average mass concentrations of BBOA in autumn (14.8 ± 5.1 μg m^{-3}) and winter (11.6 ± 6.8 μg m^{-3}) were similar, but its fractional contribution to total OA decreased from 31.9% in autumn to 15.3% in winter, due to enhanced contributions from other sources in winter. The enhanced concentrations of BBOA during the night indicated to the large emissions from residential heating. The average mass concentration of OOA and its fraction in OA increased dramatically from 9.7 ± 4.1 μg m^{-3} (20.9%) in autumn to 26.5 ± 10.4 μg m^{-3} (34.9%) in winter, likely due to enhanced emissions of precursors and stagnant meteorological conditions which facilitated the accumulation and secondary aerosol formation. Moreover, OOA concentration was heavily increased during polluted days, by a factor of 4 in autumn and factor of 6 in winter compared to clean days. In both seasons, OOA formation was dominated by photochemical oxidation under conditions of ALWC less than 30 μg m^{-3} or by aqueous-phase processes when O_x was less than 35 ppb. Back trajectory analysis indicated that the Guanzhong basin was the main source of BBOA emission, with a higher mass concentration of BBOA for air masses circulated within the Guanzhong basin (16.5-18.1 μg m^{-3}), compared to air masses from the Northwest and West

(10.9-14.5 μg m^{-3}). In addition, compared with OA sources in other regions of China, BBOA (17-19% of NR-PM_1 mass) and coal combustion OA (10-20% of NR-PM_1 mass) were major emission sources in the Guanzhong Basin and the BTH region, respectively, whereas OOA (10-34% of NR-PM_1 mass) was an important source in all studied regions.

Acknowledgement

This work was supported by the National Natural Science Foundation of China (NSFC) under Grant No. 41925015, 91644219, and 41877408, the Chinese Academy of Sciences (no. ZDBS-LY-DQC001), the Cross Innovative Team fund from the State Key Laboratory of Loess and Quaternary Geology (No. SKLLQGTD1801), the SFI-funded centre MaREI, and the Multi-Year Research Grant (No. MYRG2018-00006-FST) from University of Macau Research Council. The authors also thank Yichen Wang for assistance in field measurements.

References

Alfarra, M.R., Prévôt, A.S.H., Szidat, S., Sandradewi, J., Weimer, S., Schreiber, D., Mohr, M., Baltensperger, U., 2007. Identification of the mass spectral signature of organic aerosols from wood burning emissions. Environ. Sci. Technol. 41(16), 5770-5777.

An, Z.S., Huang, R.J., Zhang, R.Y., Tie, X.X., Li, G.H., Cao, J.J., Zhou, W.J., Shi, Z.G., Han, Y.M., Gu, Z.L., Ji, Y.M., 2019. Severe haze in northern China: A synergy of anthropogenic emissions and atmospheric processes. Proc. Natl. Acad. Sci. 116(18), 8657-8666.

Canonaco, F., Crippa, M., Slowik, J.G., Baltensperger, U., and Prévôt, A.S.H., 2013. SoFi, an Igor based interface for the efficient use of the generalized multilinear engine (ME-2) for source apportionment: application to aerosol mass spectrometer data. Atmos. Meas. Tech. 6(12), 3649-3661.

Canagaratna, M. R., Jayne, J. T., Jimenez, J. L., Allan, J. D., Alfarra, M. R., Zhang, Q., Onasch, T. B., Drewnick, F., Coe, H., Middlebrook, A., Delia, A., Williams, L. R., Trimborn, A. M., Northway, M. J., DeCarlo, P. F., Kolb, C. E., Davidovits, P., and Worsnop, D. R., 2007. Chemical and microphysical characterization of ambient aerosols with the Aerodyne aerosol mass spectrometer, Mass Spectrom. Rev. 26(2), 185–222.

Cohen, A. J., Brauer, M., Burnett, R., Anderson, H. R., Frostad, J., Estep, K., Balakrishnan, K., Brunekreef, B., Dandona, L., Dandona, R., Feigin, V., Freedman, G., Hubbell, B., Jobling, A., Kan, H. D., Knibbs, L., Liu, Y., Martin, R., Morawska, L., Pope III, C. A., Shin, H., Straif, K., Shaddick, G., Thomas, M., van Dingenen, R., van Donkelaar, A., Vos, T., Murray, C. J. L., and Forouzanfar, M. H., 2017. Estimates and 25-year trends of the global burden of disease attributable to ambient air pollution: an analysis of data from the Global Burden of Diseases Study 2015. The Lancet. 389(10082), 1907–1918.

Crippa, M., Canonaco, F., Lanz, V.A., Äijälä, M., Allan, J.D., Carbone, S., Capes, G., Ceburnis, D., Dall'Osto, M., Day, D.A., DeCarlo, P.F., Ehn, M., Eriksson, A., Freney, E., Hildebrandt Ruiz, L., Hillamo, R., Jimenez, J.L., Junninen, H., KiendlerScharr, A.,

Kortelainen, A.-M., Kulmala, M., Laaksonen, A., Mensah, A.A., Mohr, C., Nemitz, E., O'Dowd, C., Ovadnevaite, J., Pandis, S.N., Petäjä, T., Poulain, L., Saarikoski, S., Sellegri, K., Swietlicki, E., Tiitta, P., Worsnop, D.R., Baltensperger, U., Prévôt, A.S.H., 2014. Organic aerosol components derived from 25 AMS data sets across Europe using a consistent ME-2 based source apportionment approach. Atmos. Chem. Phys. 14(12), 6159-6176.

Dai. Q.L., Bi, X.H., Liu, B.S., Li, L.W., Ding, J., Song, W.B., Bi, S.Y., Schulze, B.C., Song C.B., Wu, J.H., Zhang, Y.F., Feng, Y.C., Hopke, P.K., 2018. Chemical nature of $PM_{2.5}$ and PM_{10} in Xi'an, China: Insights into primary emissions and secondary particle formation. Environmental Pollution. 240, 155-166.

DeCarlo, P.F., Ulbrich, I.M., Crounse, J., de Foy, B., Dunlea, E.J., Aiken, A.C., Knapp, D., Weinheimer, A.J., Campos, T., Wennberg, P.O., Jimenez, J.L., 2010. Investigation of the sources and processing of organic aerosol over the Central Mexican Plateau from aircraft measurements during MILAGRO. Atmos. Chem. Phys. 10(12), 5257-5280.

Duan, J., Huang, R.-J., Lin, C.S., Dai, W.T., Wang, M. Gu, Y.F., Wang, Y., Zhong, H.B., Zheng, Y., Ni, H.Y., Dusek, U., Chen, Y., Li, Y.J., Chen, Q., Worsnop, D.R., O'Dowd, C.D., Cao, J.J., 2019. Distinctions in source regions and formation mechanisms of secondary aerosol in Beijing from summer to winter. Atmos. Chem. Phys. 19(15), 10319-10334.

Du, W., Sun, Y.L., Xu, Y.S., Jiang, Q., Wang, Q.Q., Yang, W., Wang, F., Bai, Z.P., Zhao, X.D.,

Yang, Y.C., 2015. Chemical characterization of submicron aerosol and particle growth events at a national background site (3295 m a.s.l.) on the Tibetan Plateau. Atmos. Chem. Phys. 15(18), 10811-10824.

Elser, M., Huang, R.-J., Wolf, R., Slowik, J.G., Wang, Q., Canonaco, F., Li, G., Bozzetti, C., Daellenbach, K.R., Huang, Y., Zhang, R., Li, Z., Cao, J., Baltensperger, U., El-Haddad, I., Prévôt, A.S.H., 2016. New insights into $PM_{2.5}$ chemical composition and sources in two major cities in China during extreme haze events using aerosol mass spectrometry. Atmos. Chem. Phys. 16(5), 3207-3225.

He, L.-Y., Lin, Y., Huang, X.-F., Guo, S., Xue, L., Su, Q., Luan, S.-J., Zhang, Y.-H., 2010. Characterization of high-resolution aerosol mass spectra of primary organic aerosol emissions from Chinese cooking and biomass burning. Atmos. Chem. Phys. 10(23), 11535-11543.

Hu, W., Hu, M., Hu, W., Jimenez, J. L., Yuan, B., Chen, W., Wang, M., Wu, Y., Chen, C., Wang, Z., Peng, J., Zeng, L., and Shao, M., 2016. Chemical composition, sources, and aging process of submicron aerosols in Beijing: Contrast between summer and winter. J. Geophys. Res. Atmos. 121(4), 1955–1977.

Huang, R.-J., Zhang, Y.L., Bozzetti, C., Ho, K.-F., Cao, J.J., Han, Y.M., Daellenbach, K.R., Slowik, J.G., Platt, S.M., Canonaco, F., Zotter, P., Wolf, R., Pieber, S.M., Bruns, E.A., Crippa, M., Ciarelli, G., Piazzalunga, A., Schwikowski, M., Abbaszade, G., Schnelle-Kreis, J.,

Zimmermann, R., An, Z., Szidat, S., Baltensperger, U., El-Haddad, I.E., Prévôt, A.S.H., 2014. High secondary aerosol contribution to particulate pollution during haze events in China. Nature. 514(7521), 218-222.

Huang, R.-J., Wang, Y.C., Cao, J.J., Lin, C.S., Duan, J., Chen, Q., Li, Y.J., Gu, Y.F., Yan, J., Xu, W., Frohlich, R., Canonaco, F., Bozzetti, C., Ovadnevaite, J., Ceburnis, D., Canagaratna, M.R., Jayne, J., Worsnop, D.R., El-Haddad, I., Prévôt, A. S. H., O'Dowd, C.D., 2019. Primary emissions versus secondary formation of fine particulate matter in the most polluted city (Shijiazhuang) in North China. Atmos. Chem. Phys. 19(4), 2283-2298.

Huang, X.F., Xue, L., Tian, X.D., Shao, W.W., Sun, T.L., Gong, Z.H., Ju W.W., Jiang, B., Hu, M., He, L.Y., 2013. Highly time-resolved carbonaceous aerosol characterization in Yangtze River Delta of China: Composition, mixing state and secondary formation. Atmos. Environ. 64, 200–207.

Li, H.Y., Zhang, Q., Zhang, Q., Chen, C.R., Wang, L.T., Wei, Z., Zhou, S., Parworth, C., Zheng, B., Canonaco, F., Prévôt, A.S.H., Chen, P., Zhang, H.L., He, K.B., 2017. Wintertime aerosol chemistry and haze evolution in an extremely polluted city of North China Plain: significant contribution from coal and biomass combustions. Atmos. Chem. Phys. 17(7), 4751-4768.

Li, Y.J., Lee, B.P., Su, L., Fung, J.C.H., Chan, C.K., 2015. Seasonal characteristics of fine

particulate matter (PM) based on high-resolution time-of-flight aerosol mass spectrometric (HR-ToF-AMS) measurements at the HKUST Supersite in Hong Kong. Atmos. Chem. Phys. 15(1), 37-53.

Liu, P.P., Zhang, Y.L., Wu, T.T., Shen, Z.X., Xu, H.M., 2019. Acid-extractable heavy metals in $PM_{2.5}$ over Xi'an, China: seasonal distribution and meteorological influence. Environ Sci Pollut Res. 26(33), 34357-34367.

Middlebrook, A.M., Bahreini, R., Jimenez, J.L., Canagaratna, M.R., 2012. Evaluation of composition-dependent collection efficiencies for the aerodyne aerosol mass spectrometer using field data. Aerosol Sci. Tech. 46(3), 258-271.

Massoli, P., Fortner, E. C., Canagaratna, M. R., Williams, L. R., Zhang, Q., Sun, Y., Schwab, J. J., Trimborn, A., Onasch, T. B., Demerjian, K. L., Kolb, C. E., Worsnop, D. R., and Jayne, J. T., 2012. Pollution Gradients and Chemical Characterization of Particulate Matter from Vehicular Traffic Near Major Roadways: Results from the 2009 Queens College Air Quality Study in NYC. Aerosol Sci. Tech. 46(11), 1201–1218.

Ng, N. L., Canagaratna, M. R., Jimenez, J. L., Zhang, Q., Ulbrich, I. M., and Worsnop, D. R., 2011. Real-time methods for estimating organic component mass concentrations from aerosol mass spectrometer data. Environ. Sci. Technol. 45(3), 910-916.

Paatero, P. and Tapper, U., 1994. Positive Matrix Factorization: a nonnegative factor model with optimal utilization of error estimates of data values. Environmetrics. 5(2), 111-126.

Paatero, P., 1997. Least squares formulation of robust non-negative factor analysis. Chemom. Intell. Lab. 37(1), 23-35.

Paatero, P., 1999. The multilinear engine: a table-driven, least squares program for solving multilinear problems, including the n-way parallel factor analysis model. J. Comput. Graph. Stat. 8(4), 854-888.

Sun, Y.L., Wang, Z., Fu, P., Jiang, Q., Yang, T., Li, J., Ge, X., 2013a. The impact of relative humidity on aerosol composition and evolution processes during wintertime in Beijing, China. Atmos. Environ. 77, 927-934, 2013a.

Sun, Y.L., Wang, Z.F., Fu, P.Q., Yang, T., Jiang, Q., Dong, H.B., Li, J., Jia, J.J., 2013b. Aerosol composition, sources and processes during wintertime in Beijing, China. Atmos. Chem. Phys. 13(9), 4577-4592.

Sun, Y., Du, W., Fu, P., Wang, Q., Li, J., Ge, X., Zhang, Q., Zhu, C., Ren, L., Xu, W., Zhao, J., Han, T., Worsnop, D.R., Wang, Z., 2016a. Primary and secondary aerosols in Beijing in winter: sources, variations and processes. Atmos. Chem. Phys. 16(13), 8309-8329.

Sun, C., Lee, B.P., Huang, D., Jie Li, Y., Schurman, M.I., Louie, P.K.K., Luk, C., Chan, C.K., 2016b. Continuous measurements at the urban roadside in an Asian megacity by Aerosol Chemical Speciation Monitor (ACSM): particulate matter characteristics during fall and winter seasons in Hong Kong. Atmos. Chem. Phys. 16(3), 1713-1728.

Sun, Y.L., Xu, W.Q., Zhang, Q., Canonaco, F., Prévôt, A.S.H, Fu, P.Q., Li, J., Jayne, J., Worsnop, D.R., and Wang, Z.F., 2018. Source apportionment of organic aerosol from 2-year highly time-resolved measurements by an aerosol chemical speciation monitor in Beijing, China. Atmos. Chem. Phys. 18(12), 8469–8489.

Tie, X., Huang, R.-J., Dai, W.T., Cao, J.J., Long, X., Su, X.L., Zhao, S.Y., Wang, Q.Y., Li, G.H., 2016. Effect of heavy haze and aerosol pollution on rice and wheat productions in China. Sci. Rep. 6(1), 29612.

Wang, P., Cao, J.J., Shen, Z.X., Han, Y.M., Lee, S.C., Huang, Y., Zhu, C.S., Wang, Q.Y., Xu, H.M., Huang, R.-J., 2015a. Spatial and seasonal variations of $PM_{2.5}$ mass and species during 2010 in Xi'an, China. Science of the Total Environment. 508, 1, 477-487.

Wang, Q., Sun, Y., Jiang, Q., Du, W., Sun, C., Fu, P., and Wang, Z., 2015b. Chemical composition of aerosol particles and light extinction apportionment before and during the heating season in Beijing, China. J. Geophys. Res. Atmos. 120(24), 12708-12722.

Wang, Y.C., Huang,R.-J., Ni, H.Y., Chen, Y., Wang, Q.Y., Li, G.H., Tie, X.X., Shen, Z.X., Huang, Y., Liu, S.X., Dong, W.M., Xue, P., Frohlich, R., Canonaco, F., Elser, M., Daellenbach, K.R., Bozzetti, C., El-Haddad, I., Prévôt, A.S.H., Canagaratna, M.R., Worsnop, D.R., Cao, J.J., 2017. Chemical composition, sources and secondary processes of aerosols in Baoji city of northwest China. Atmos. Environ. 158, 128-137.

Xu, H.M., Ho, S.S.H, Cao, J.J., Guinot, B., Kan, H.D., Shen, Z.X., Ho, K.F., Liu, S.X., Zhao, Z.Z., Li, J.J., Zhang, N.N., Zhu, C.S., Zhang, Q., Huang, R.-J. 2017, A 10-year observation of PM($_{2.5}$)-bound nickel in Xi'an, China: Effects of source control on its trend and associated health risks. Sci. Rep., 7, 41132.

Zhang, Y.J., Tang, L.L., Yu, H.X., Wang, Z., Sun, Y.L., Qin W., Chen, W.T., Chen, C.H., Ding, A.J., Wu, J., Ge, S., Chen, C., Zhou, H.C., 2015a. Chemical composition, sources and evolution processes of aerosol at an urban site in Yangtze River Delta, China during wintertime. Atmos. Environ. 123, 339-349.

Zhang, Y.W., Zhang, X.Y., Zhang, Y.M., Shen, X.J., Sun, J.Y., Ma, Q.L., Yu, X.M., Zhu, J.L., Zhang, L., Che, H.C., 2015b. Significant concentration changes of chemical components of PM_1 in the Yangtze River Delta area of China and the implications for the formation mechanism of heavy haze–fog pollution. Science of the Total Environment, 538, 7-15.

Zhang, Y.J., Tang, L.L., Wang, Z., Yu, H.X., Sun, Y.L., Liu, D., Qin, W., Canonaco, F., Prev ot,

A.S.H., Zhang, H.L., Zhou, H.C., 2015c. Insights into characteristics, sources, and evolution of submicron aerosols during harvest seasons in the Yangtze River Delta region, China. Atmos. Chem. Phys. 15(3), 1331-1349.

Zheng, Y., Cheng, X., Liao, K., Li, Y., Li, Y.J., Huang, R.-J., Hu, W., Liu, Y., Zhu, T., Chen, S., Zeng, L., Worsnop, D.R., Chen, Q., 2020. Characterization of Anthropogenic Organic Aerosols by TOF-ACSM with the New Capture Vaporizer. Atmos. Meas. Tech., 13(5), 2457-2472.

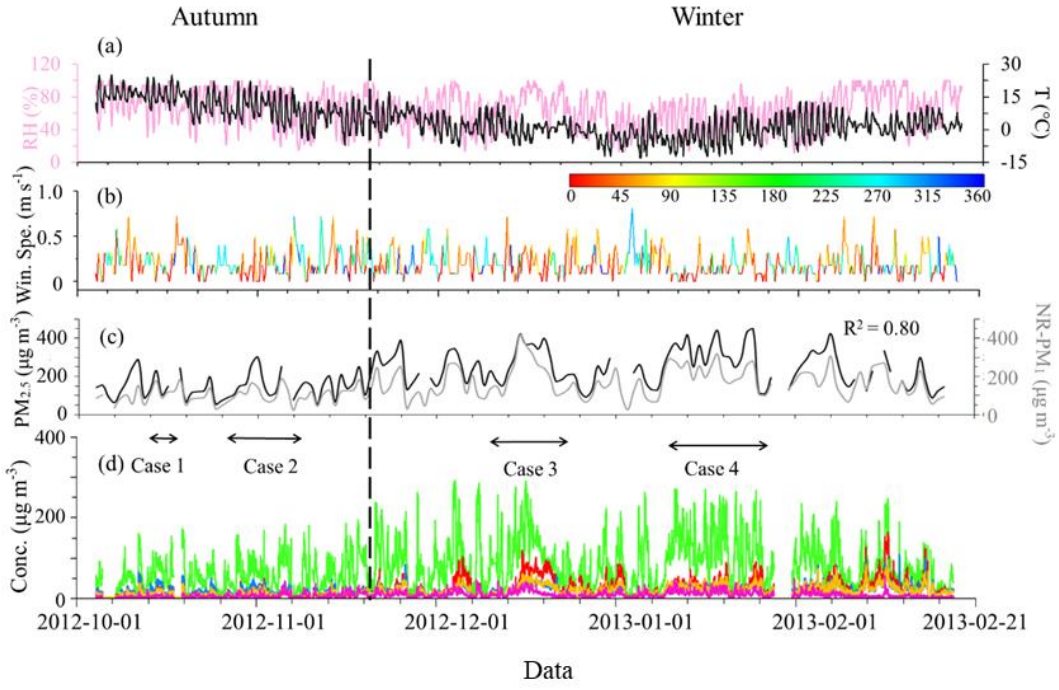

Figure 1. Time series of (a) RH and temperature, (b) wind speed and wind direction, (c) concentration of $PM_{2.5}$ and NR-PM_1, and (d) concentration of NR-PM_1 species (organic, sulphate, nitrate, ammonium and chloride) for the observation period Black dotted line is set on the 15th of Nov to separate the study period into autumn (former) and winter (latter). Four pollution episodes are selected for case study.

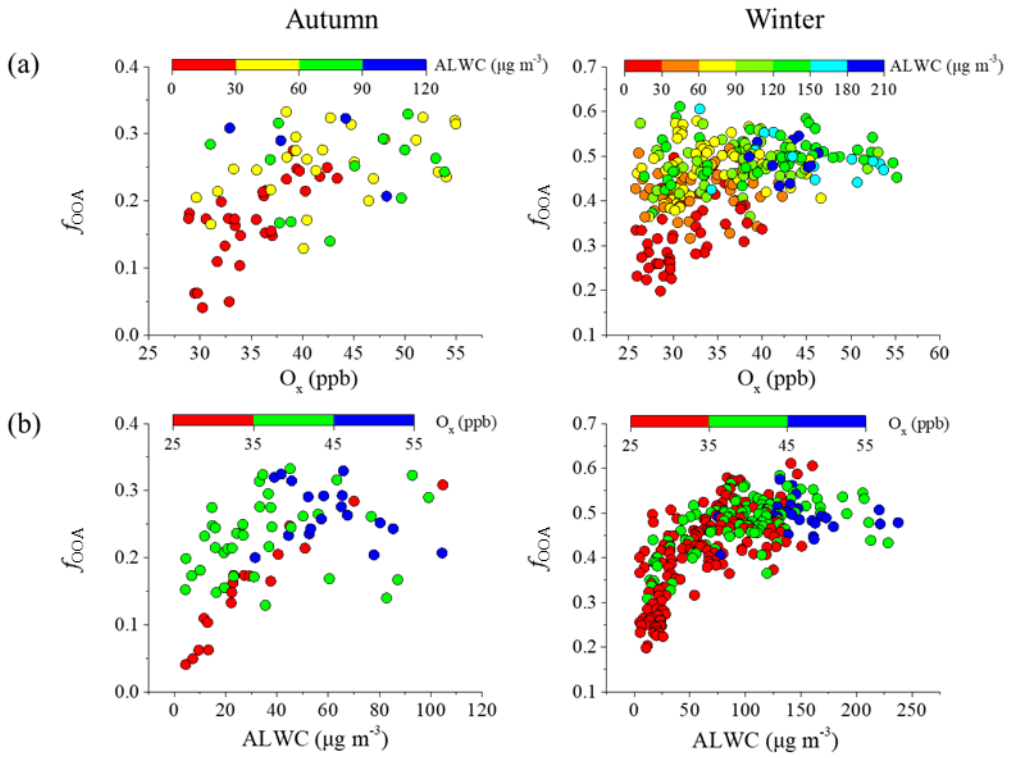

Figure 2. Scatter plots of (a) f_{OOA} versus O_x concentration and (b) f_{OOA} versus ALWC concentration in autumn and winter. Data are color coded by the corresponding (a) ALWC concentration and (b) O_x concentration, respectively. Nighttime (19:00-6:00) was not included in the analysis.

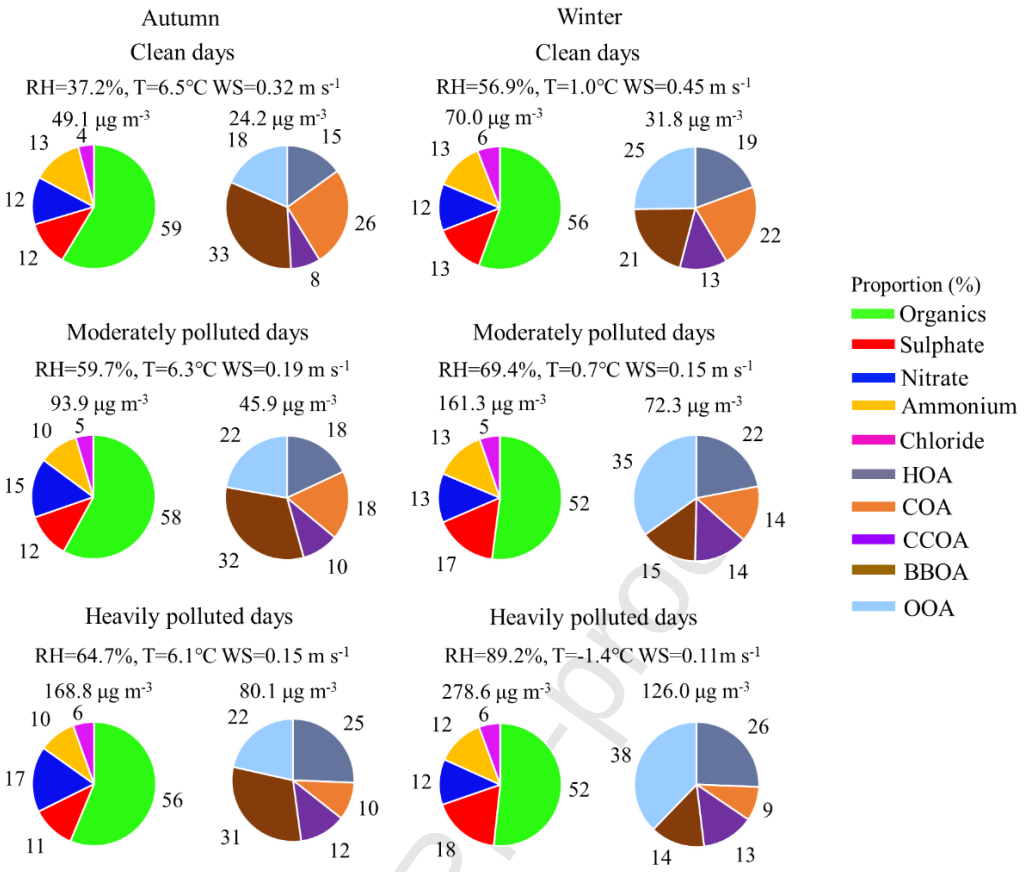

Figure 3. Sources apportionment results of NR-PM_1 species and OA factors in clean days, moderately polluted days and heavily polluted days during autumn and winter. Three pollution conditions were defined as the 25th, 25-75th and 75th percentiles of NR-PM_1 daily average mass concentration respectively.

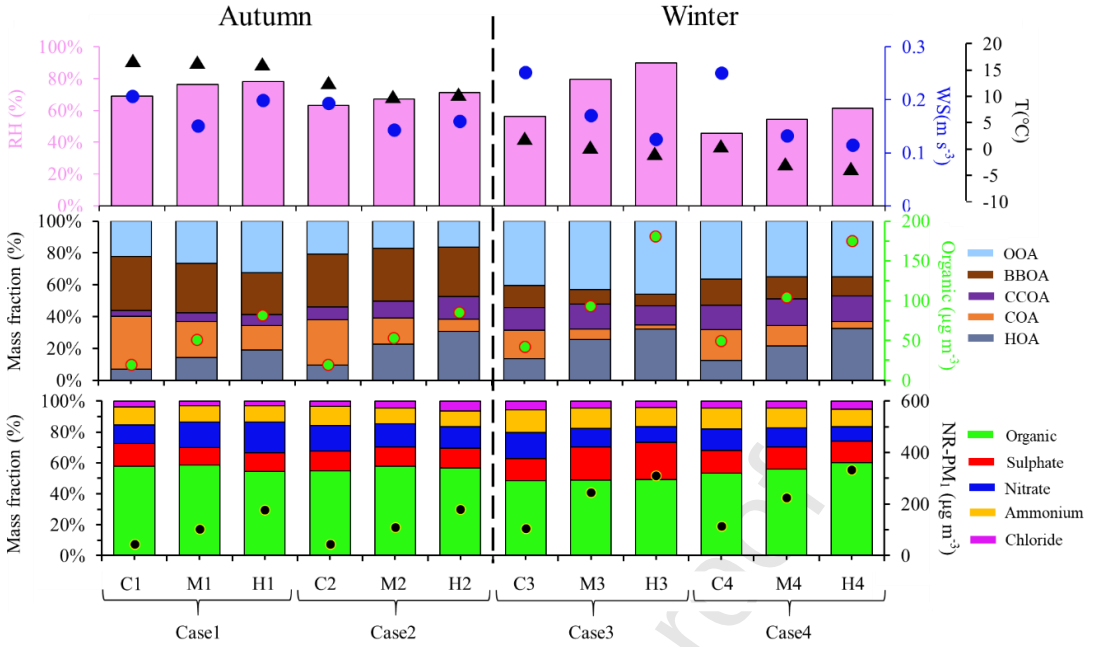

Figure 4. Bar chart comparison of meteorological parameters (including relative humidity, wind speed and temperature), OA factors, and NR-PM_1 species for four cases. C1-C4, M1-M4 and H1-H4 represent clean days, moderately polluted days and heavily polluted days respectively. The black and green dots indicate the average mass concentration of NR-PM_1 and total OA for each period, respectively. Black dotted line is used to separate autumn and winter period.

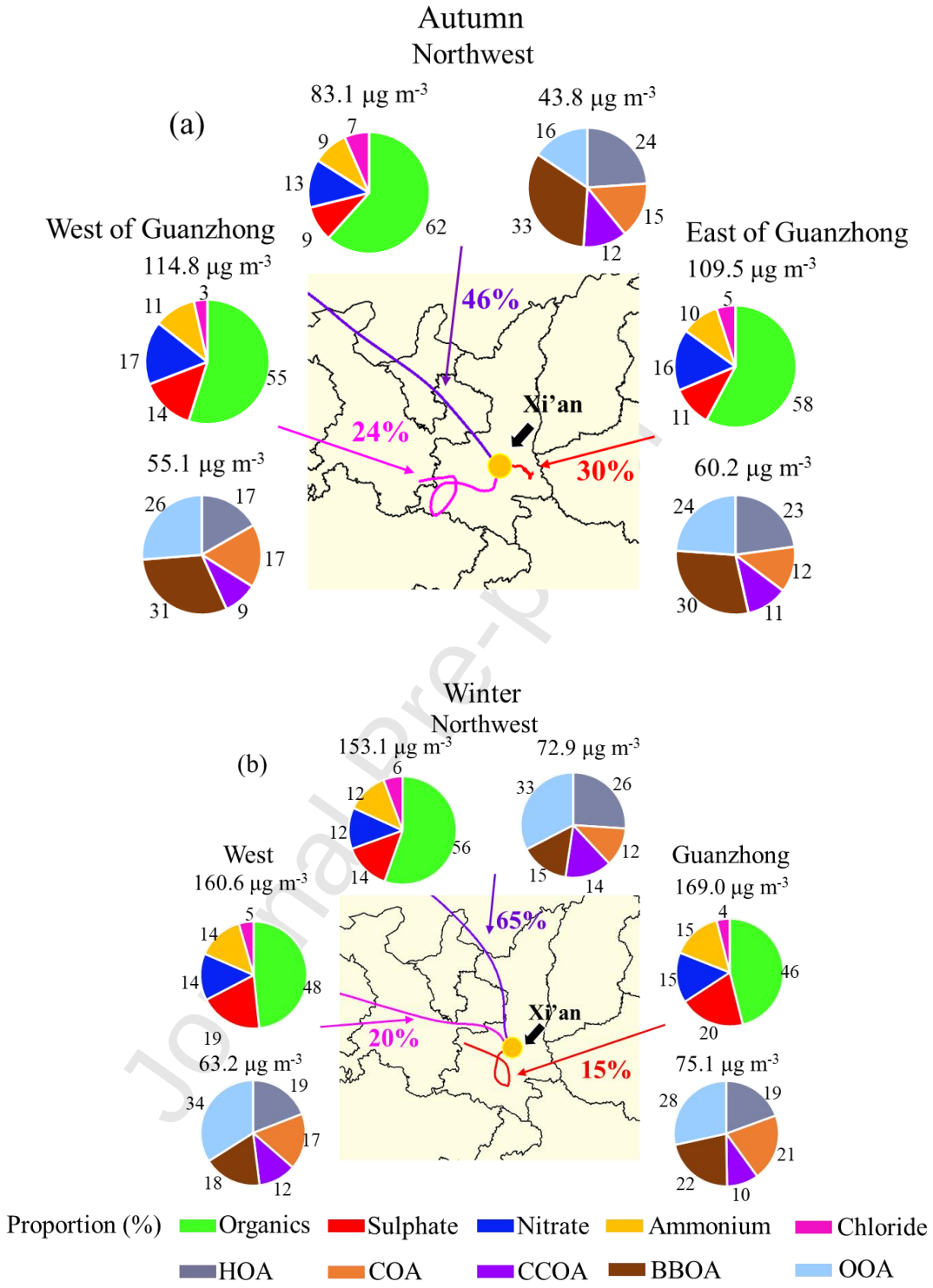

Figure 5. The trajectories at 500 m height were calculated per hour using HYSPLIT model in TrajStat. Three air mass clusters according to trajectories cluster analysis during autumn (a) (Northwest, West of Guanzhong, and East of Guanzhong) and winter (b) (Northwest, West,

and Guanzhong) were shown, with their NR-PM_1 species and OA factors.

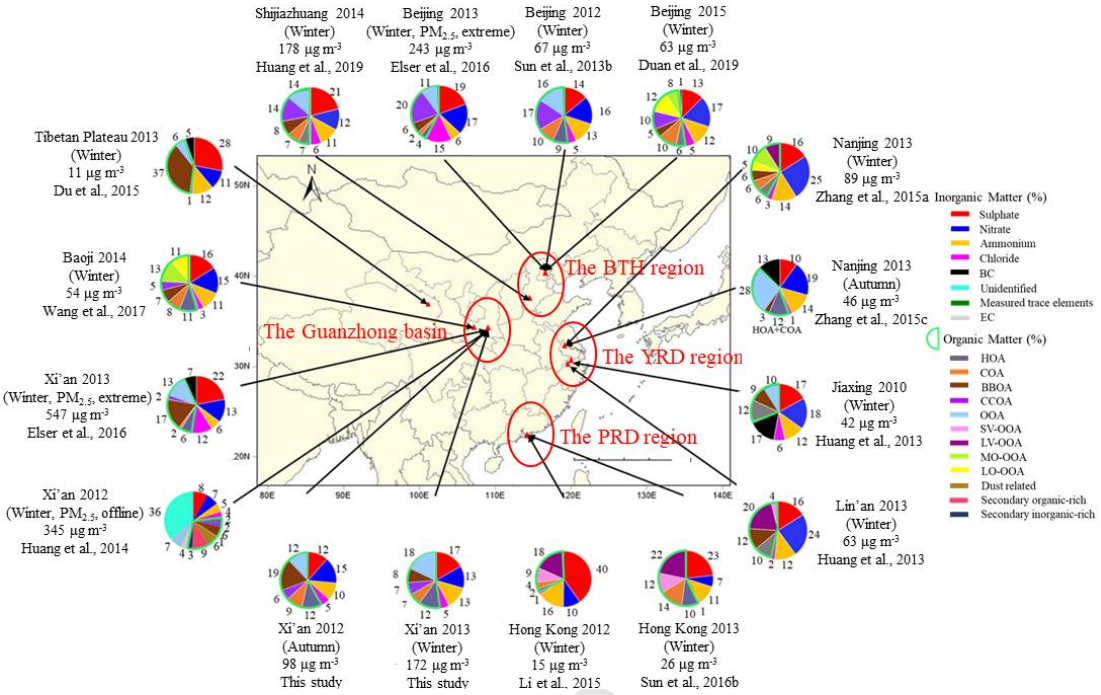

Figure 6. Comparison of NR-PM_1 composition and OA sources in different regions of China, measured by AMS/ACSM between 2010 and 2015. These data are from Xi'an (Huang et al., 2014; Elser et al., 2016), Baoji (Wang et al., 2017), Beijing (Sun et al., 2013b; Elser et al., 2016; Duan et al., 2019), Shijiazhuang (Huang et al., 2019), Nanjing (Zhang et al., 2015a; Zhang et al., 2015c), Jiaxing (Huang et al., 2013), Lin'an (Zhang et al., 2015b), Hong Kong (Li et al., 2015; Sun et al., 2016b) and Tibetan Plateau (Du et al., 2015). Of note, the particle sizes of Elser et al. (2016) and Huang et al. (2014) are NR-$PM_{2.5}$ and $PM_{2.5}$.

Conflict of interest Statement

We declare that the manuscript entitled "**Seasonal variations in the sources of organic aerosol in Xi'an, Northwest China: the importance of biomass burning and secondary formation**" is original, has not been full or partly published before, and is not currently being considered for publication elsewhere.

We confirm that the manuscript has been read and approved by all named authors and that there are no other persons who satisfied the criteria for authorship but are not listed. We further confirm that the order of authors listed in the manuscript has been approved.

We understand that the Corresponding Author is the sole contact for the editorial process. The corresponding author "Ru-Jin Huang" is responsible for communicating with the other authors about process, submissions of revisions, and final approval of proofs."

Credit author statement

HBZ and RJH designed the study. Data analysis and source apportionment were done by HBZ. HBZ wrote the Original Draft. JD, CSL and RJH wrote the Review & Editing. All authors commented on and discussed the manuscript.

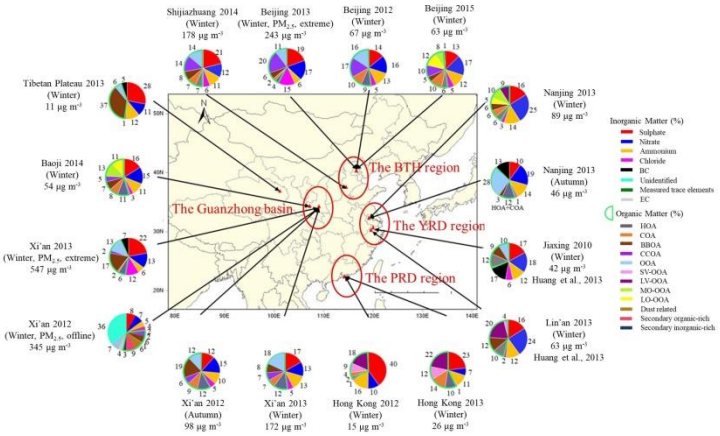

Graphical abstract

Highlights

- Biomass burning and secondary formation dominated OA in both autumn and winter in Xi'an
- OOA formation was dominated by photochemical or aqueous-phase processes under different conditions
- BBOA and CCOA were major sources in the Guanzhong Basin and the BTH region, respectively